The Astrophysical Journal, 979:239 (10pp), 2025 February 1 https://doi.org/10.3847/1538-4357/ada1c2

Detection of Enhanced Germanium in a New Cool Extreme Helium Star A980: Insights and Implications

Ajay Kumar Saini[1,2] and Gajendra Pandey[1]
[1] Indian Institute of Astrophysics, II Block, Koramangala, Bengaluru-560034, Karnataka, India; ajay.saini@iiap.res.in
[2] Pondicherry University, R.V. Nagar, Kalapet, Pondicherry-605014, UT of Puducherry, India
Received 2024 November 18; revised 2024 December 16; accepted 2024 December 16; published 2025 January 29

Abstract

A fine abundance analysis of a recently discovered hydrogen-deficient carbon (HdC) star, A980, is presented. Based on the observed high-resolution optical spectrum, we ascertain that A980 is a cool extreme helium (EHe) star and not an HdC star. Singly ionized germanium Ge II lines are identified in A980's optical spectrum. These are the first-ever detections of germanium lines in an EHe star's observed spectrum and provide the first measurements of germanium abundance in an EHe star. The overabundance of germanium in A980's atmosphere provides us with evidence for the synthesis of germanium in EHe stars. Among the known cool EHe stars, A980 exhibits a maximum enhancement of the *s*-process elements based on a significant number of transitions. The measured elemental abundances reveal signs of H-burning, He-burning, and specifically the nucleosyntheses of the key elements Ge, Sr, Y, Zr, and Ba. The nucleosyntheses of these key elements are discussed in light of asymptotic giant branch evolution and the expectation from the accretion of an He white dwarf by a C–O white dwarf or by a neutron star.

Unified Astronomy Thesaurus concepts: Hydrogen deficient stars (769); Chemically peculiar stars (226); Helium-rich stars (715); Chemical abundances (224); Nucleosynthesis (1131)

Materials only available in the online version of record: machine-readable table

1. Introduction

There exists a distinct category of hydrogen-deficient stars that have enhanced carbon features and diminished hydrogen Balmer lines in their observed spectra compared with those expected for their effective temperatures. This was first pointed out by W. P. Bidelman (1953).

W. P. Bidelman (1953) listed four stars in this category, and these are not light or photometric variables.[3] B. Warner (1963) included one more star, HD 148839, in this category of nonvariables. Note that the observed spectrum of HD 148839 shows the usual presence of enhanced C_2 bands and C I lines, and the absence of a CH band, although not very weakened Balmer lines.

Until the year 2022, there were just these five known in this category and termed hydrogen-deficient carbon (HdC) stars. Earlier, B. Warner (1967) conducted an abundance analysis of these five stars to investigate their surface composition. A recent survey has reported 27 new HdC stars based on their low-resolution spectra—about a sixfold increase in their number over those known earlier (P. Tisserand et al. 2022). Detailed abundance analysis serves as a crucial observational constraint on theoretical models concerning the formation and evolution of these peculiar stars.

In this paper we conduct an abundance analysis of a new warm HdC star, A980 (2MASS 18113561+0154326), using a high-resolution spectrum.

2. Observations, Data Reduction, and Line Identification

We have obtained a high-resolution optical spectrum of the newly identified warm HdC star A980 using the Hanle Echelle Spectrograph (Sriram et al. 2018) mounted on the 2 m Himalayan Chandra Telescope at the Indian Astronomical Observatory (IAO) in Hanle, Ladakh, India. These observations were made on 2023 June 21. The spectrum was recorded onto a 4k × 4k CCD that covered the wavelength range from 3856 to 9656 Å with a resolving power ($R = \lambda/\Delta\lambda$) of about 30,000. A total of three frames, each of 45 minute exposure, were observed and coadded to improve the signal-to-noise ratio (ranging from 25 to 180 per pixel across the covered spectral range from blue to red). A Th–Ar hollow cathode lamp was observed for wavelength calibration. To normalize the pixel-to-pixel variation in the sensitivity of the CCD, several exposures known as flat frames with differing spectrograph focus (in focus and out of focus) were acquired using a featureless quartz–halogen lamp. All the flat frames were combined to create a master flat with a very high signal for flat correction. A telluric standard—a rapidly rotating B-type bright star—was also observed on the same night to get rid of Earth's atmospheric absorption lines. The observed spectrum of the star was then reduced utilizing the standard tasks under the Image Reduction and Analysis Facility (IRAF) software package (D. Tody 1986, 1993). In IRAF, the task `telluric` is used to remove Earth's atmospheric absorption lines by dividing the observed telluric standard spectrum from the observed spectrum of our program star.

[3] Notably, there exists yet another class of hydrogen-deficient stars known as R Coronae Borealis (RCB) stars. RCB stars exhibit remarkable photometric variability by undergoing an unpredictable decline in light (by up to about 9 mag in visual) in a matter of a few weeks and recover gradually to their maximum light in several months (G. C. Clayton 1996).

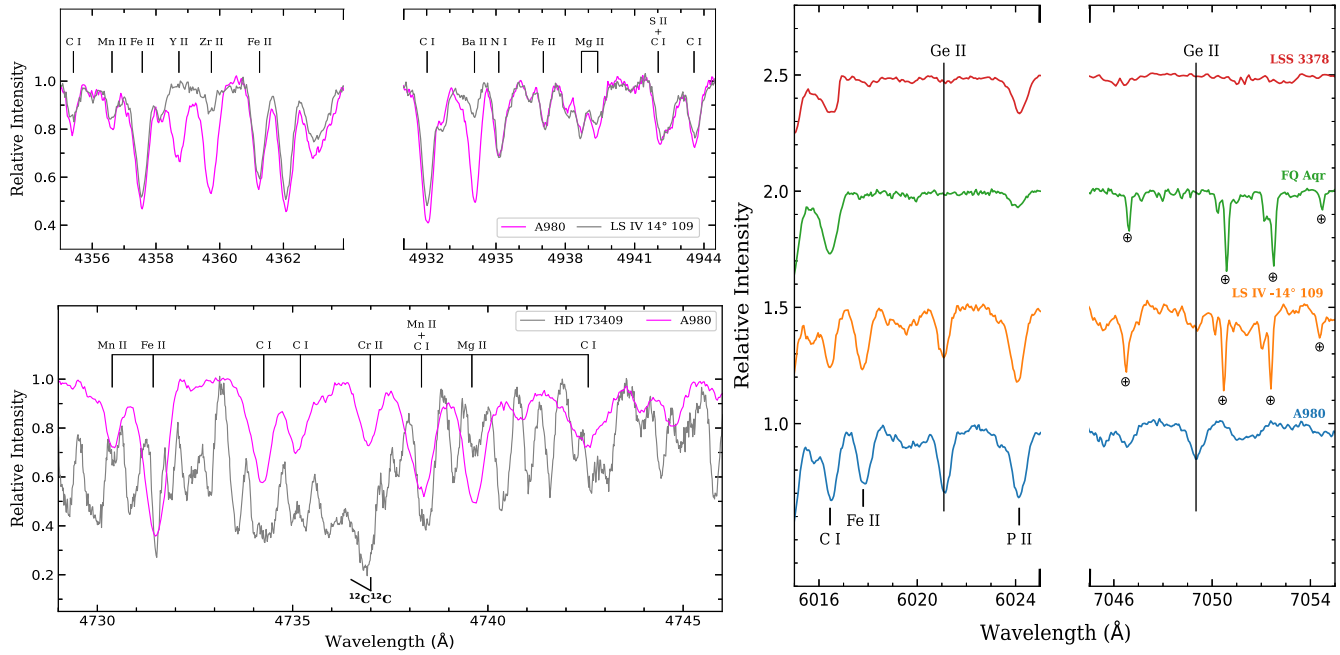

Figure 1. Observed spectra of LS IV −14°109, a known cool EHe star, and A980 are shown for comparison in the top left panel. Observed spectra of HD 173409, a known HdC star, and A980 in the region of the (1, 0) C_2 band are shown for comparison in the bottom left panel. In the right panel, identification of Ge II λ6021.04 and λ7049.37 lines in A980 and the other cool EHe stars LS IV −14°109, FQ Aqr, and LSS 3378 are highlighted by vertical lines. The principal lines are marked. The telluric absorption lines are shown by encircled crosses. A key is provided on each panel.

For the spectral line identifications, we have used the NIST Atomic Spectra Database,[4] A Multiplet Table of Astrophysical Interest—revised edition (C. E. Moore 1972), Tables of Spectra of H, C, N, and O (C. E. Moore 1993), Kurucz's database,[5] and the VALD database.[6] A large spectral coverage (3856–9656 Å) of the star's observed spectrum has enabled us to identify several important elements with their significant number of lines, about 1900, and their ionization stages. The observed absorption line spectrum is well represented by neutral helium lines, neutral and singly ionized carbon lines, and also by plenty of singly ionized metal lines of the iron group.[7] Singly ionized helium is not detected in the spectrum. Lines of all elements expected and observed in early A-type and late B-type normal stars are found. The observed spectrum exhibits remarkably diminished hydrogen Balmer lines and the absence of C_2 molecular features. We note that the above-described characteristics fit well with the observed absorption lines of an extreme helium (EHe) star, especially the cooler EHe stars (G. Pandey et al. 2001). A comparison with the available high-resolution spectrum of the cool EHe star, LS IV −14°109, reveals that the observed spectrum of the program star A980 is a near replica of the former except for the significantly enhanced absorptions of neutron-capture elements in A980's spectrum (see Figure 1, top left panel, for example). The presence of an He I line in the observed spectrum of A980 is also shown along with that of LS IV −14°109 in Figure 2(d). The observed spectrum of an HdC star, HD 173409 (available from B. P. Hema et al. 2012), when compared with that of A980, shows the absence of the C_2 molecular features in A980 (see Figure 1, bottom left panel, for example). These comparisons clearly demonstrate that A980 is not an HdC star. However, P. Tisserand et al. (2022) have classified A980 as a warm HdC star and have renamed the category of HdC stars as dustless HdC stars.

Among the several absorptions of the neutron-capture elements in A980's spectrum, the most notable were the identifications of singly ionized germanium Ge II lines.

2.1. Ge II Lines

Only two multiplets are listed in the Revised Multiplet Table (RMT; C. E. Moore 1972) for the identification of Ge II lines. Of the two Ge II lines of RMT 1, the line at 6021.09 Å is clearly present in A980's spectrum, while the stronger line at 5893.42 Å is severely blended as it is engulfed by a strong Na D_1 component from the interstellar medium. No Ge II lines of RMT 2 are detected in the observed spectrum. However, the NIST Atomic Spectra Database provides more multiplets that include the above-discussed two multiplets listed in the RMT for further line identification. A thorough search was made for all Ge II lines of these multiplets. Two more unblended Ge II lines, λ7049.37 and λ7145.39, from multiplet ^2D–$2P^0$ of transition array $4s4p^2$–$4s^25p$ were identified; the third line λ6966.32 of this multiplet is severely contaminated by an Fe II line. The Ge II line λ6021.09 that was identified using the RMT is from multiplet ^2S–$2P^0$ of transition array $4s^25s$–$4s^25p$. We note that Ge II lines from the multiplets of the excited levels with lower excitation potentials (LEPs) of 9.7 eV or higher make a negligible contribution to the observed spectrum of A980. We also searched for Ge II lines in the available spectra of three cooler EHe stars: LS IV −14°109, FQ Aqr, and LSS 3378 (see G. Pandey et al. 2001; G. Pandey & B. E. Reddy 2006). All the Ge II lines that were detected in A980's spectrum are also present in the available spectrum of LS IV −14°109. Along with these detected lines, the spectrum of LS IV −14°109 revealed an additional unblended line

[4] See https://physics.nist.gov/asd.
[5] See http://kurucz.harvard.edu.
[6] See https://vald.astro.uu.se.
[7] The radial velocity of A980, determined from the identified Fe II lines, is measured to be 109 ± 2 km s^{-1}.

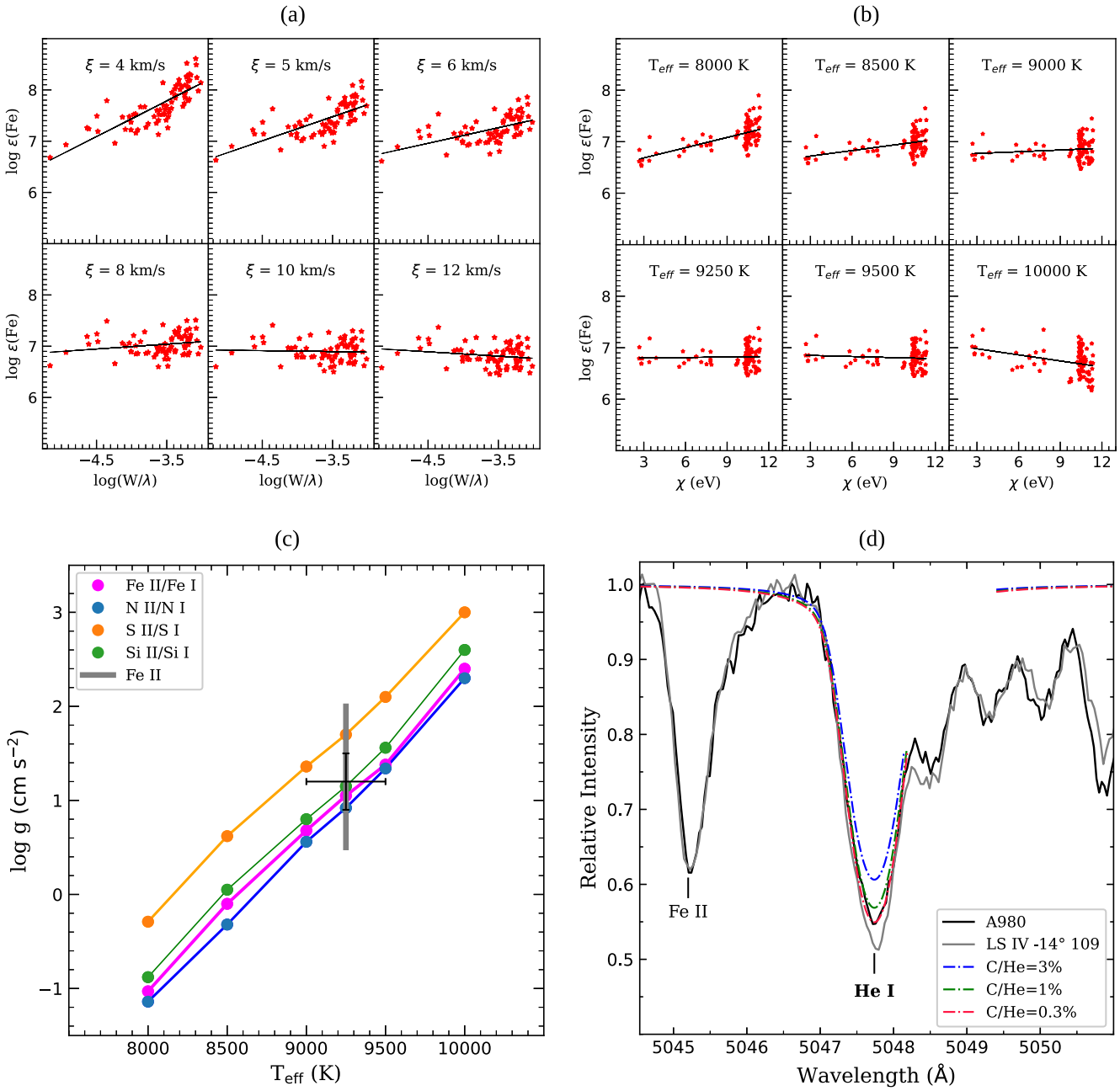

Figure 2. (a) Abundances from Fe II lines for A980 vs. their reduced equivalent widths $\log(W_\lambda/\lambda)$. A value of $\xi = 11.0$ km s^{-1} is obtained from this figure. (b) Abundances from Fe II lines for A980 vs. their lower excitation potential (χ), showing excitation equilibrium. A value of $T_{\rm eff} = 9250 \pm 250$ K is obtained from this figure. (c) The ($T_{\rm eff}$, log g) plane of A980 shows the final values of $T_{\rm eff}$ and log g with error bars. Loci satisfying ionization equilibria are plotted—see keys on the figure. The excitation equilibrium of Fe II lines is shown by the thick solid gray line. (d) Synthesized and observed He I λ5047.74 profiles. The He I line profiles are synthesized using the model $T_{\rm eff} = 9250$ K, log $g = 1.25$ (cgs), and $\xi = 11.5$ km s^{-1} for three different values of C/He. The observed He I λ5047.74 profile of LS IV $-14°109$ is also shown for comparison. A key is provided on each panel.

λ5893.39, the strongest line from the multiplet RMT 1, ^2S–$2P^0$, which was expected to be present in A980's spectrum but was severely contaminated as discussed earlier. Our search for all the above identified Ge II lines, including the strongest line at 5893.39 Å, in the available spectra of the other two cool EHe stars, FQ Aqr and LSS 3378, was unsuccessful (for example, see the right panel of Figure 1).

3. Abundance Analysis—Procedure

The procedure for abundance analysis involves predicting the observed spectrum using a grid of model atmospheres combined with a radiative transfer code in local thermodynamic equilibrium (LTE). The predictions of an observed spectrum were made in the sense of computing the line equivalent width or synthesizing the line spectrum.

3.1. Hydrogen-deficient Model Atmospheres

For the analysis of A980, a cool EHe star, the same procedure is followed as described by G. Pandey et al. (2001). The abundance analysis uses two grids of line-blanketed hydrogen-deficient model atmospheres, one with $T_{\rm eff} \leqslant 9500$ K and the other with $T_{\rm eff} \geqslant 10{,}000$ K. The grid

with $T_{\rm eff} \leqslant 9500$ K, the Uppsala line-blanketed models, is described by M. Asplund et al. (1997), and that with $T_{\rm eff} \geqslant 10{,}000$ K was computed by the code STERNE (C. S. Jeffery & U. Heber 1992). The line-formation calculations, which involve computing the line equivalent width as well as the spectrum synthesis using the Uppsala models, were carried out with the Uppsala LTE line-formation code EQWIDTH. Similarly, the spectrum synthesis code SYNSPEC (I. Hubeny & T. Lanz 2017) was adopted for the line-formation calculations using STERNE as well as Uppsala models.

3.2. Consistency between Line-formation Codes and between Model Grids

For an adopted model atmosphere, the abundances derived using SYNSPEC and EQWIDTH for weak lines are in good agreement within 0.1 dex for a majority of the species. We notice that the abundances derived using the former are always lower than those derived using the latter. We attribute these small differences to the adopted continuous opacity data being from two different sources.

>The two model atmosphere grids, as discussed above, do not overlap in effective temperature. These two grids are compared by deriving a model for 9500 K using extrapolation of the high-temperature grid whose coolest models are at 10,000 K. The extrapolated model and an Uppsala model for 9500 K gave identical abundances to within 0.05 dex (G. Pandey et al. 2001).

3.3. Atomic Data

The *gf*-values and excitation potentials for most of the lines used in our LTE analysis were available in the NIST database. The data for the remaining lines are from the Kurucz database and other sources (see Appendix B: Table B1). However, for several Zr II lines, we have used new improved experimental *gf*-values from the compilations of G. Ljung et al. (2006) and G. Malcheva et al. (2006). The Stark broadening and radiation broadening coefficients are mostly from the Kurucz database. The line broadening coefficients for computing the He I profiles are from M. S. Dimitrijevic & S. Sahal-Brechot (1984). The line broadening treatments for synthesizing hydrogen Balmer lines are from I. Hubeny et al. (1994) as used by SYNSPEC. See Table B1 for the detailed line list used in our analysis.

3.4. Atmospheric Parameters and Elemental Abundances

A model atmosphere is characterized by its effective temperature, surface gravity, and chemical composition. The input elemental abundances of the adopted model atmosphere need to be consistent with those derived from the observed spectrum. A model atmosphere of an EHe star is mainly governed by the input carbon and helium abundances. Specifically, both carbon and helium are the major contributors to the continuum opacity in cool EHe stars (G. Pandey et al. 2001). Hence, the input C/He ratio of the adopted model atmosphere needs to be in accord with that determined from the star's observed spectrum. The input composition of the rest of the elements is scaled to solar with H/He fixed at 10^{-4} by number.

A fine abundance analysis starts with deriving the star's effective temperature ($T_{\rm eff}$), surface gravity ($\log g$), and the microturbulent velocity (ξ). Subsequently, the photospheric elemental abundances are estimated for the adopted model atmosphere. These parameters are determined from the observed line spectrum.

The microturbulent velocity ξ (in km s^{-1}) is first determined by imposing that the lines of a particular species, neutral or ionized, with similar LEP and having a range in their measured equivalent widths, return the same abundance.

Second, the condition of ionization balance needs to be satisfied, i.e., an element represented in the observed spectrum by neutral as well as the ionized states must return the same abundance from lines of different stages of ionization. This designates a locus in the ($T_{\rm eff}$, $\log g$) plane. Such elements with their pairs of ions provide loci of very similar slope in the ($T_{\rm eff}$, $\log g$) plane.

The third condition that needs to be satisfied is the excitation balance, which serves as a thermometer measuring $T_{\rm eff}$. This requires that the lines of a particular species but of differing LEPs should return the same elemental abundance. The model grid is searched for the model that meets this condition. The optimum $T_{\rm eff}$ is found to be independent of the adopted $\log g$ and C/He for the model atmosphere. Hence, this indicator provides a locus in the ($T_{\rm eff}$, $\log g$) plane to lift the degeneracy presented by the ionization balance. A second indicator may be available: for stars hotter than about 10,000 K, the He I profiles are less sensitive to $T_{\rm eff}$ than to $\log g$ on account of pressure broadening due to the quadratic Stark effect.

In reproducing the observed spectrum by spectrum synthesis, we include broadening due to the instrumental line profiles and the microturbulent velocity ξ, and assign all additional broadening, if any, to rotational broadening. Observed unblended line profiles, preferably weak, are used to obtain the additional broadening. The synthetic line profile, including the broadening due to the instrumental profile, for the adopted model atmosphere ($T_{\rm eff}$, $\log g$, ξ) and the abundance (from equivalent width analysis) is found to be sharper than the observed line profiles. This extra broadening in the observed profile is attributed to rotational broadening.

4. A980—Results of Abundance Analysis

A test model atmosphere is adopted with $T_{\rm eff} = 9500$ K, $\log g = 1.0$, and C/He = 1% to first determine the microturbulent velocity ξ. These stellar parameters were chosen due to the nearly identical observed spectra of A980 and LS IV $-14°109$ (see Section 2). The stellar parameters derived for LS IV $-14°109$ by G. Pandey et al. (2001) are the same as adopted above. ξ is determined from lines of Fe II, Ti II, Cr II, and C I. ξ is found to be 11.0 km s^{-1} from Fe II and Ti II lines, 12.0 km s^{-1} from Cr II lines, and 11.5 km s^{-1} from C I lines. We finally adopt a mean ξ of 11.5 $\pm$ 1.0 km s^{-1} for determining the elemental abundances. For example, see Figure 2(a), which illustrates the procedure of estimating ξ.

$T_{\rm eff}$ was obtained from Fe II lines that exhibit a range in their LEPs: 2 to 11 eV. For $\xi = 11.5$ km s^{-1}, we found a model ($T_{\rm eff}$, $\log g$, ξ) that provided the same abundance independent of the line's LEP. $T_{\rm eff}$ deduced from the Fe II lines has negligible dependence on the adopted model's $\log g$ and C/He ratio. Figure 2(b) illustrates the procedure for obtaining $T_{\rm eff}$.

The loci obtained from the ionization balance of Fe II/Fe I, N II/N I, Si II/Si I, and S II/S I are shown in Figure 2(c). These combined with $T_{\rm eff}$ deduced from the excitation balance of Fe II lines, which has negligible dependence on surface gravity, eventually provide the optimum stellar parameters: $T_{\rm eff} = 9250 \pm 250$ K, $\log(g/{\rm cm\ s^{-2}}) = 1.2 \pm 0.3$, and $\xi = 11.5 \pm 1.0$ km s^{-1}.

For the derived stellar parameters, the C/He ratio may directly be determined from the measured equivalent widths of C I and C II lines. The observed He I line profiles are presumably yet another indicator of the C/He ratio. Figure 5 of G. Pandey et al. (2001) illustrates the predicted equivalent widths of C I, C II, and He I lines for a model's C/He ratio. At the derived $T_{\rm eff}$ and $\log g$ of A980, the predicted C I line strengths are insensitive to the model's C/He $\geqslant 1.0\%$; C/He of 1% corresponds to a carbon abundance of $\log \epsilon({\rm C}) = 9.5$. However, the C II line strengths are nearly insensitive to the model's C/He $\geqslant 0.3\%$. The observed C II lines are very strong and the measured equivalent widths are very large. Hence, we conclude that C II lines are not fit for estimating the C/He ratio and instead use C I lines for determining it.

The C I lines return carbon abundances of $\log \epsilon({\rm C}) = 8.9 \pm 0.2$, 9.0 ± 0.2, and 9.3 ± 0.2 for the optimum model's input ratio of C/He = 0.3% ($\log \epsilon({\rm C}) = 9.0$), 1.0% ($\log \epsilon({\rm C}) = 9.5$), and 3.0% ($\log \epsilon({\rm C}) = 10.0$), respectively. We find that the input model's carbon abundance is consistent with that derived for the optimum model with a C/He of 0.3%. He I profiles at 5048, 5876, and 6678 Å may provide an estimate of the C/He ratio. The best fitting observed profile of He I is shown in Figure 2(d). A ratio C/He of about 0.3% produces an acceptable fit to the He I profile. Within the uncertainties, which are mainly line-to-line scatter, a ratio C/He = 0.3% is determined from the C I lines as well as the He I profiles independently.

The final abundances, as given in Table 1, are derived for the optimum model of C/He = 0.3%. The derived abundances are normalized based on the convention that $\log \epsilon({\rm X}) = \log({\rm X/H}) + 12.0$ to a scale in which $\log \sum \mu_I \epsilon(I) = 12.15$, where 12.15 is determined from solar abundances with He/H $\simeq 0.1$. Here, $\mu_{\rm X}$ is the atomic weight of element X. Since all elements but He have a very low abundance, the helium abundance $\log \epsilon({\rm He})$ is 11.54 on this scale. The hydrogen abundance is from the syntheses of Hα, Hβ, and Hγ profiles, for example, see Figure C1 in the Appendix. Neutral lines of the key element fluorine are also present in the spectrum of A980 like in other cool EHe stars (G. Pandey 2006). Fluorine abundance is determined by spectrum syntheses of neutral fluorine (F I) lines (see Figure 3, bottom panels). The abundance of germanium, a very significant element for this study, is from spectrum syntheses of Ge II lines at 6021.04, 7049.37, and 7145.39 Å (see Figure 3, top panels). The deduced projected rotational velocity ($v \sin i$) of about 15 km s^{-1} is adopted for spectrum syntheses.

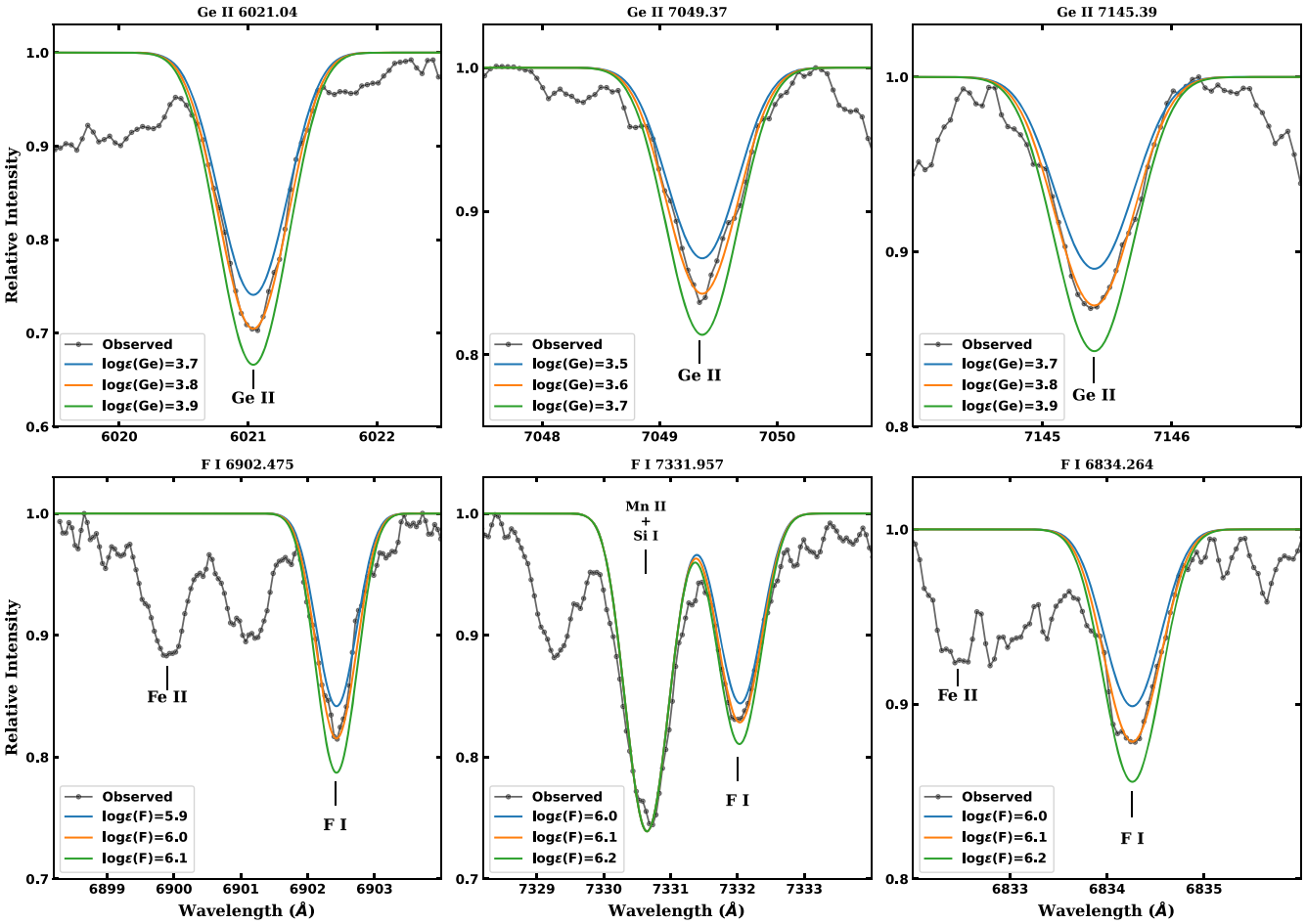

Figure 3. For A980, top and bottom panels show the spectrum syntheses of Ge II and F I lines, respectively. See the key on each panel.

Table 1
Derived Elemental Abundances for A980 and LS IV −14°109

Element	Solar[a]	A980[b]		LS IV −14°109[c]	
	log ϵ(X)	log ϵ(X)	[X/Fe]	log ϵ(X)	[X/Fe]
H	12	5.81	−5.39	6.20	−5.30
He	10.93	11.54	⋯	11.54	⋯
C	8.43	8.87	1.24	9.45	1.52
N	7.83	8.40	1.37	8.60	1.27
O	8.69	7.89	0.00	8.50	0.31
F	4.56	6.10	2.34	6.52	2.46
Ne	7.93	8.65	1.52	9.40	1.97
Na	6.24	6.46	1.02	6.80	1.06
Mg	7.60	7.00	0.20	7.20	0.10
Al	6.45	6.14	0.49	6.90	0.95
Si	7.51	7.30	0.59	7.68	0.67
P	5.41	5.36	0.75	5.30	0.39
S	7.12	6.89	0.57	7.55	0.93
Ar	6.40	5.99	0.39	⋯	⋯
Ca	6.34	5.64	0.10	5.55	−0.29
Sc	3.15	2.98	0.63	3.30	0.65
Ti	4.95	4.27	0.12	4.30	−0.15
V	3.93	3.40	0.27	⋯	⋯
Cr	5.64	4.75	−0.09	5.10	−0.04
Mn	5.43	4.85	0.22	5.30	0.37
Fe	7.50	6.70	0.00	7.00	0.00
Co	4.99	4.72	0.53	⋯	⋯
Ni	6.22	5.50	0.08	5.92[d]	0.20
Ge	3.65	3.72	0.87	3.48[b]	0.33
Sr	2.87	3.40	1.33	2.60	0.23
Y	2.21	2.54	1.13	1.90	0.19
Zr	2.58	2.93	1.15	1.90	−0.18
Ba	2.18	2.23	0.85	1.70	0.02

Notes. [X/Fe] = $(X/Fe)_{\star} - (X/Fe)_{\odot}$.
[a] Solar abundances are adopted from M. Asplund et al. (2009).
[b] This work.
[c] Adopted from G. Pandey et al. (2001) and G. Pandey (2006).
[d] From the unblended cleaner lines and their adopted *gf*-values used in this work for A980.

The inclusion of hyperfine splitting (hfs) makes a negligible difference in the derived elemental abundances of our program star. For example, an abundance of Ba II λ4934.10 returns the same value within 0.1 dex when derived using hfs components. We also note that the synthesized Ba II λ4934.10 line profile without including hfs components is a better fit to the observed line profile.

5. Surface Composition—Discussion

The derived surface composition of A980 is summarized in Table 1 along with that of the comparison star LS IV −14°109 (G. Pandey et al. 2001); also given are the solar abundances from M. Asplund et al. (2009). The derived abundances of the cool EHe star A980 are then compared with the measured abundances of other EHe stars from the literature (see G. Pandey et al. 2021 and references therein).

The surface composition of A980 clearly reveals that its atmosphere is hydrogen-poor and rich in helium and carbon as observed for most of the EHe stars. These are clues that the atmosphere of A980 is contaminated by the products of H- and He-burning reactions.

For the evolved low- and intermediate-mass stars, abundances of elements that are unlikely to be affected by H- and He-burning and attendant nuclear reactions are good indicators of their initial metallicity. Such elements are V, Cr, Mn, Fe, Co, and Ni—the iron-peak elements, and Mg, Si, S, Ca, Sc, and Ti—the α-elements. We note that A980's abundance ratios, Mg/Fe, Si/Fe, S/Fe, Ca/Fe, Sc/Fe, V/Fe, Cr/Fe, Mn/Fe, Co/Fe, and Ni/Fe, are on average as expected for metal-poor normal and unevolved stars (see Table 1; A. Goswami & N. Prantzos 2000; N. Ryde & D. L. Lambert 2004). We adopt iron abundance as the indicator of initial metallicity in A980.

The elements whose abundances are affected in the course of A980's evolution are H, He, C, N, O, F, Ne, Ge, Sr, Yr, Zr, and Ba when compared to a normal star, for example, the Sun—see Table 1.

We discuss by comparing the derived surface composition of A980 with that of other EHe stars. The surface compositions of other EHe stars including the hot RCB star DY Cen are from C. S. Jeffery & U. Heber (1992), J. S. Drilling et al. (1998), C. S. Jeffery (1998, 2017), C. S. Jeffery et al. (1998, 2024), G. Pandey et al. (2001, 2004, 2006, 2014), G. Pandey (2006), G. Pandey & B. E. Reddy (2006), G. Pandey & D. L. Lambert (2011, 2017), and A. Bhowmick et al. (2020).

Hydrogen. The hydrogen abundance log ϵ(H) is found to be 5.8 ± 0.2, which is underabundant by a factor of ~10^6 relative to a normal star. A980's hydrogen abundance fits well within the range of 5−8 that is derived for other EHe stars (see G. Pandey et al. 2021 and references therein). The exceptions are the hot RCB, DY Cen, and the EHe stars with a very low carbon abundance (see the following section).

Carbon. The carbon abundance log ϵ(C) is found to be 8.9 ± 0.2, which equates to a C/He ratio of 0.0023. A980 falls at the lower end of the range of C/He ratios in other EHe stars. Here we exclude the four known EHe stars with a very low carbon abundance. However, recent studies suggest that HD 144941, one of these four, is the most extreme helium-strong star with an extremely strong magnetic field (see N. Przybilla et al. 2021; M. E. Shultz et al. 2021).

Nitrogen. Nitrogen abundance is enriched by a factor of 25 (1.4 dex) relative to the expected initial abundance for A980's metallicity, which is the Fe abundance. The enhanced nitrogen abundance shows the complete conversion of initial C, N, and O to N. This provides evidence for the operation of severe CNO cycling in an H-rich region.

Oxygen. Oxygen abundance is close to the initial value expected for A980's Fe abundance. The O/N ratio is found to be 0.94 for A980 and is in concert with the other EHe stars having an O abundance close to their initial value (see G. Pandey et al. 2006).

Fluorine. Fluorine abundance is significantly enhanced, by about a factor of 200 when compared with the F expected for A980's metallicity. This enhancement is in concert with other cool and hot EHe stars including the RCB stars (see A. Bhowmick et al. 2020).

Neon. Neon abundances are from Ne I lines and are subject to non-LTE effects. Application of the non-LTE effects most likely brings the Ne abundances of the cool EHe stars, here A980 (down by about 0.8 dex), in line with those of the hot EHe stars (G. Pandey & D. L. Lambert 2011).

Germanium. The germanium abundance log ϵ(Ge), derived from spectrum synthesis, is 3.7 ± 0.1. Relative to iron, Ge is overabundant with respect to solar by about a factor of 8 (0.9 dex). This provides the first measurement of germanium abundance in EHe stars.

Table 2
Surface Abundance Ratios for Comparative Analysis

	A980[a]	CO+He[b]	AGB[c]		
			2.5 $M_\odot$	5 $M_\odot$ (VW93)	5 $M_\odot$ (B95)
[Fe]	−0.80	−1.55	−0.70	−0.70	−0.70
[Ge/Fe]	+0.87	⋯	+0.50	+0.90	+0.30
[Ge/ls]	−0.34	⋯	−1.10	−0.10	+0.10
[Ge/hs]	+0.02	⋯	−1.80	+0.50	+0.25
[ls/hs]	+0.36	+0.50	−0.70	+0.60	+0.15
[Sr/Fe]	+1.33	⋯	+1.50	+1.10	+0.25
[Y/Fe]	+1.13	+1.35	+1.60	+1.05	+0.20
[Zr/Fe]	+1.15	+0.95	+1.70	+0.95	+0.15
[Ba/Fe]	+0.85	+0.65	+2.30	+0.40	+0.05

Notes.
[a] This work.
[b] Adopted from A. Menon et al. (2019): Case 1 predictions.
[c] Adopted from A. I. Karakas et al. (2018).

Strontium, Yr, Zr, and Ba. Relative to iron, Sr, Yr, Zr, and Ba are found to be overabundant with respect to solar by factors of about 20 (1.3 dex), 13 (1.1 dex), 16 (1.2 dex), and 8 (0.9 dex), respectively. A980 provides a maximum enhancement of *s*-process elements measured in a cool EHe star to date using a significantly reliable number of transitions—these are 4, 12, 16, and 4 for Sr, Yr, Zr, and Ba, respectively.

6. Discussion and Conclusions

A fine abundance analysis based on A980's observed high-resolution spectrum clearly demonstrates that it is a cool EHe star.

The surface abundances of A980 are measured especially for the key elements: CNO, fluorine, and the heavier elements: Ge, Sr, Y, Zr, and Ba. The measured C/He ratio is about 0.2% and is the lowest known. Note that the other EHe stars, excluding the four known EHe stars with a very low carbon abundance, exhibit a range in their C/He ratios of 0.3%−1.3%.

EHe stars are thought to be products of double white dwarf mergers. Case 1 predictions from Figure 5 of A. Menon et al. (2019) for CO+He white dwarf mergers are in broad agreement with the observed abundances of A980, in particular the enhanced fluorine and the *s*-process elements (Y, Zr, Ba), compared to solar.

A significant addition is the determination of germanium abundance in two cool EHe stars, A980 and LS IV −14°109, with similar stellar parameters ($T_{\rm eff}$, log g). These are the first determination of Ge abundances in EHe stars. The atmosphere of A980 is significantly enhanced in germanium, that is, 8 times higher than the solar value relative to iron. This notable enhancement is evidence of the synthesis of germanium in the cool EHe star A980. Note that A980 is enriched by about a factor of 4 in germanium (Ge/Fe) relative to LS IV −14°109 while A980's enrichment in germanium is about a factor of 16 when compared with the normal subgiant HD 107113 of similar metallicity; HD 107113's Ge and Fe abundances are from I. U. Roederer (2012).

Two primary processes that could account for the synthesis of germanium are first the neutron-capture process (A. I. Karakas et al. 2007 and references therein) and second the rapid proton-capture process, known as the *rp*-process (G. T. Biehle 1994). Knowledge of the germanium production mechanism in A980 will provide new clues to the origin of EHe stars. To identify the process of germanium production, A980's observed abundances of Ge, light *s*-process (Sr, Y, Zr), and heavy *s*-process (Ba) elements were compared with predictions from A. I. Karakas et al. (2018) for low- to intermediate-mass asymptotic giant branch (AGB) stars (see Table 2). A980's mass is estimated to be $1 \pm 0.5\ M_\odot$ based on its luminosity, which is calculated using the absolute magnitude from P. Tisserand et al. (2022), along with our derived surface gravity (g) and effective temperature ($T_{\rm eff}$). For AGB stars, as given in Table 2, the abundance ratios are shaped by *s*-process nucleosynthesis. The expected ratios for a low-mass AGB star (2.5 $M_\odot$) are [Ge/Fe] = +0.5, [Ge/ls] = −1.1, and [ls/hs] = −0.7. However, for A980, the observed ratios are notably different: [Ge/Fe] = +0.87, [Ge/ls] = −0.34, and [ls/hs] = +0.36. Here, ls and hs represent the light and heavy *s*-process abundances, respectively. Specifically, the ratio [ls/hs] > 0 in A980 contradicts predictions for low-mass AGB stars where heavy *s*-process elements are expected to be more abundant. The expected ratios for an intermediate-mass AGB star (5 $M_\odot$), with different mass loss rates, VW93 and B95, are provided in Table 2 (see A. I. Karakas et al. 2018 for VW93 and B95). Here, the ratio [ls/hs] > 0 for both cases and is in line with that observed for A980. The abundance ratios for the mass loss rate VW93 are found to be in fair agreement with that observed for A980. This suggests that the atmosphere of A980 is contaminated by germanium produced via the *s*-process taking place in an intermediate-mass AGB star. Note that the abundance ratios depend on the adopted mass loss rate for intermediate-mass AGB stars but nucleosynthesis processes remain the same.

In comparison, the observed abundance ratios do suggest that the atmosphere of LS IV −14°109 is not contaminated by freshly synthesized Ge and *s*-process elements (see Table 1).

Alternatively, a significant enhancement in germanium abundance is evident from Thorne–Żytkow objects (TŻOs) and presumably produces elements via the rapid proton-capture process (*rp*-process). TŻOs are proposed as the possible merged products of a neutron star and a nondegenerate star. R. Farmer et al. (2023) provide recent predictions of surface abundance ratios for TŻOs but those are not in the regime of A980's metallicity and helium fraction to perform a comparative analysis.

The abundance ratios [ls/Fe] and [hs/Fe] for A980 are similar to the predictions for CO+He white dwarf mergers (A. Menon et al. 2019). However, predictions of germanium abundances are not available for CO+He white dwarf mergers to explore the origin of germanium in EHe stars. Theoretical studies for germanium synthesis in CO+He white dwarf mergers need to be explored.

Acknowledgments

We thank the referee for a constructive review. This research was supported by the Science and Engineering Research Board (SERB), DST, India through grant CRG/2021/000108. A.K.S. expresses gratitude to Sriram Krishna for his assistance with installing and running SYNSPEC. He also thanks Fayaz S. and B. P. Hema for helping with the installation of the radiative transfer code EQWIDTH.

We thank the staff of IAO, Hanle, CREST, and Hosakote, who made these observations possible. The facilities at IAO and CREST are operated by the Indian Institute of Astrophysics, Bangalore.

Table A1
Errors in Elemental Abundances due to Uncertainties in the Stellar Parameters

Species	$\Delta T_{\rm eff} = +250$ (K)	$\Delta\log g = +0.25$ (cgs)	$\Delta\xi = +1.0$ (km s^{-1})	rms
C I	+0.12	−0.06	−0.03	0.13
C II	−0.17	+0.08	−0.15	0.24
N I	+0.08	−0.03	−0.02	0.09
N II	−0.12	+0.06	−0.03	0.14
O I	+0.06	−0.02	−0.05	0.08
Ne I	−0.16	+0.10	−0.09	0.21
Na I	+0.12	−0.06	−0.04	0.14
Mg I	+0.23	−0.10	−0.03	0.25
Mg II	+0.03	0.00	−0.01	0.03
Al II	−0.10	+0.07	−0.08	0.15
Si I	+0.15	−0.06	0.00	0.16
Si II	−0.08	+0.06	−0.05	0.11
P II	−0.09	+0.09	−0.03	0.13
S I	+0.13	−0.06	−0.01	0.14
S II	−0.09	+0.07	−0.05	0.13
Ca II	+0.14	−0.05	−0.02	0.15
Sc II	+0.23	−0.03	−0.01	0.23
Ti II	+0.17	−0.01	−0.04	0.17
V II	+0.14	+0.02	−0.02	0.14
Cr II	+0.08	+0.03	−0.04	0.09
Mn II	+0.06	+0.04	−0.02	0.07
Fe I	+0.21	−0.08	−0.01	0.22
Fe II	−0.01	+0.04	−0.03	0.05
Co II	+0.04	+0.05	−0.03	0.07
Ni I	+0.17	−0.07	0.00	0.18
Ni II	0.00	+0.05	−0.03	0.06
Ge II	+0.05	+0.12	+0.04	0.14
Sr II	+0.25	−0.05	−0.18	0.30
Y II	+0.26	−0.04	−0.03	0.27
Zr II	+0.21	−0.02	−0.03	0.22
Ba II	+0.26	−0.06	−0.05	0.27

Note. The abundance error due to $\Delta T_{\rm eff}$ is the difference in abundances derived from the adopted model ($T_{\rm eff}$, log g, ξ) and a model ($T_{\rm eff} + \Delta T_{\rm eff}$, log g, ξ). The abundance error due to $\Delta\log g$ is the difference in abundances derived from the adopted model ($T_{\rm eff}$, log g, ξ) and a model ($T_{\rm eff}$, log g+$\Delta\log g$, ξ). The abundance error due to $\Delta\xi$ is the difference in the abundances derived from the adopted model ($T_{\rm eff}$, log g, ξ) and a model ($T_{\rm eff}$, log g, $\xi + \Delta\xi$).

Appendix A
Error Analysis

The adopted stellar parameters are accurate to typically $\Delta T_{\rm eff} = \pm 250$ K, $\Delta\log(g/\text{cm s}^{-2}) = \pm 0.3$, and $\Delta\xi = \pm 1.0$ km s^{-1}. The line-to-line scatter (standard deviation resulting from multiple lines of the same ion) and the uncertainty in stellar parameters are the major sources of errors in deriving abundances. The abundance errors due to uncertainty in the stellar parameter are given in Table A1. Typically, the error due to uncertainty in the stellar parameter was found to be less than the line-to-line scatter. An abundance derived from more lines is always better and more reliable than one derived from fewer lines. However, this has a negligible effect on the mean abundance of element E. Therefore, we also include a weight due to the number of lines from which the ion's abundance is derived. The mean abundance of an element E was calculated as

$$\langle \text{E} \rangle = \frac{\langle \text{E}_a \rangle + \langle \text{E}_b \rangle}{2}$$

where $\langle \text{E}_a \rangle$ and $\langle \text{E}_b \rangle$ are mean abundances of an element E, calculated by giving weight due to line-to-line scatter and number of lines respectively. They are defined as

$$\langle \text{E}_a \rangle = \frac{w_{1a}\langle \text{E I} \rangle + w_{2a}\langle \text{E II} \rangle + \ldots}{w_{1a} + w_{2a}}$$

where $\langle \text{E I} \rangle$, $\langle \text{E II} \rangle$, … are the abundances derived from neutral, singly ionized, ... lines of element E. w_{1a}, w_{2a}, … are weights due to line-to-line scatter of ions (δ(E I), δ(E II), …), i.e.,

$$w_1 = \frac{1}{(\delta(\text{E I}))^2}.$$

And,

$$\langle \text{E}_b \rangle = \frac{w_{1b}\langle \text{E I} \rangle + w_{2b}\langle \text{E II} \rangle + \ldots}{w_{1b} + w_{2b}}$$

where w_{1b}, w_{2b}, … are weights due to the number of lines used to derive the abundance of ions, i.e.,

$$w_{1b} = \text{ number of lines used to derive } \langle \text{E I} \rangle.$$

Appendix B
Lines Used for Abundance Analysis

The lines used for the abundance analysis of A980 are given in Table B1. The abundance errors due to line-to-line scatter are also tabulated. Also, the LEP (χ), log gf, equivalent width (W_λ), and abundance (log ϵ) derived for each line are listed. The elemental abundances are derived by using model atmospheres with $T_{\rm eff} = 9250$ K, $\log(g/\text{cm s}^{-2}) = 1.25$, C/He = 0.3%, and microturbulent velocity $\xi = 11.5$ km s^{-1}.

Table B1
Lines Used to Derive Elemental Abundances for A980

Ion					
λ (Å)	χ (eV)	log gf	W_λ (mÅ)	log ϵ[a]	References[b]
H I					
6562.82	10.20	0.710	Synth.	5.62	NIST
4861.33	10.20	−0.020	Synth.	5.80	NIST
4340.47	10.20	−0.447	Synth.	6.00	NIST
Mean:	⋯	⋯	⋯	5.81 ± 0.16	⋯
He I					
5048.00	21.22	−1.587	Synth.	11.54	NIST
C I					
6595.24	8.85	−2.400	104	8.84	NIST
6591.45	8.85	−2.400	101	8.82	NIST
6683.95	8.85	−2.230	216	9.16	NIST
6688.79	8.85	−2.130	188	8.95	NIST
6711.29	8.86	−2.690	95	9.09	NIST
7022.24	8.64	−2.670	114	9.05	NIST

Notes.
[a] Normalized such that log $\sum \mu_i \epsilon(i) = 12.15$.
[b] Sources of log gf values.

References: NIST: A. Kramida et al. (2023); K88: R. Kurucz (1988); CC: C. R. Cowley & C. H. Corliss (1983); FMW: J. R. Fuhr et al. (1988); GARZ: T. Garz (1973); Luck: Compilations by R. E. Luck; Tom97: J. Tomkin et al. (1997); KP: R. L. Kurucz & E. Peytremann (1975); NBS: W. L. Wiese et al. (1966); Kurucz: Kurucz Database; Malcheva: G. Malcheva et al. (2006); Ljung: G. Ljung et al. (2006).
(This table is available in its entirety in machine-readable form in the online article.)

Appendix C
Spectrum Synthesis of Hydrogen Lines

The available hydrogen Balmer lines (Hα, Hβ, and Hγ) are synthesized to obtain the hydrogen abundance (log ϵ(H)). For example, synthesis of the Hα line is shown in Figure C1. The hydrogen Balmer lines are synthesized using the optimum model atmosphere with $T_{\rm eff}$ = 9250 K, log g = 1.25 cgs, ξ = 11.5 km s^{-1}, and C/He = 0.3%.

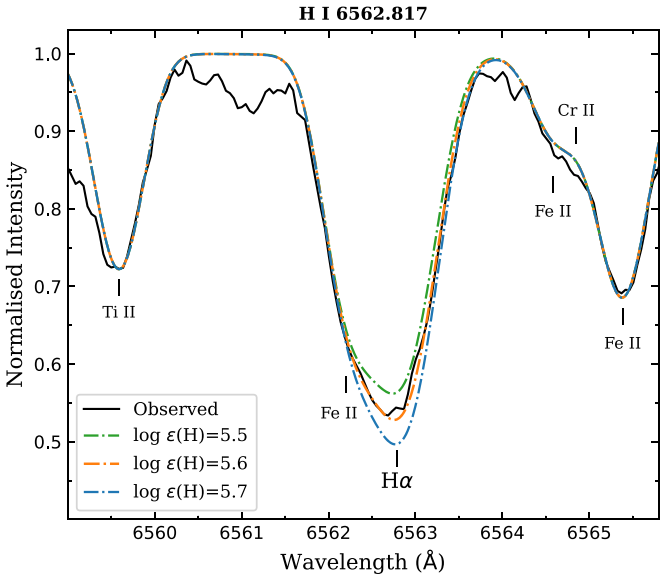

Figure C1. Observed and synthesized Hα line profiles for A980.

ORCID iDs

Ajay Kumar Saini https://orcid.org/0009-0000-6371-907X
Gajendra Pandey https://orcid.org/0000-0001-5812-1516

References

Asplund, M., Grevesse, N., Sauval, A. J., & Scott, P. 2009, ARA&A, 47, 481
Asplund, M., Gustafsson, B., Kiselman, D., & Eriksson, K. 1997, A&A, 318, 521
Bhowmick, A., Pandey, G., & Lambert, D. L. 2020, ApJ, 891, 40
Bidelman, W. P. 1953, ApJ, 117, 25
Biehle, G. T. 1994, ApJ, 420, 364
Clayton, G. C. 1996, PASP, 108, 225
Cowley, C. R., & Corliss, C. H. 1983, MNRAS, 203, 651
Dimitrijevic, M. S., & Sahal-Brechot, S. 1984, JQSRT, 31, 301
Drilling, J. S., Jeffery, C. S., & Heber, U. 1998, A&A, 329, 1019
Farmer, R., Renzo, M., Götberg, Y., et al. 2023, MNRAS, 524, 1692
Fuhr, J. R., Martin, G. A., & Wiese, W. L. 1988, JPCRD, 17
Garz, T. 1973, A&A, 26, 471
Goswami, A., & Prantzos, N. 2000, A&A, 359, 191
Hema, B. P., Pandey, G., & Lambert, D. L. 2012, ApJ, 747, 102

Hubeny, I., Hummer, D. G., & Lanz, T. 1994, A&A, 282, 151
Hubeny, I., & Lanz, T. 2017, arXiv:1706.01859
Jeffery, C. S. 1998, MNRAS, 294, 391
Jeffery, C. S. 2017, MNRAS, 470, 3557
Jeffery, C. S., Hamill, P. J., Harrison, P. M., & Jeffers, S. V. 1998, A&A, 340, 476
Jeffery, C. S., & Heber, U. 1992, A&A, 260, 133
Jeffery, C. S., Scott, L. J. A., Philip Monai, A., Miszalski, B., & Woolf, V. M. 2024, MNRAS, 530, 1666
Karakas, A. I., Lugaro, M., Carlos, M., et al. 2018, MNRAS, 477, 421
Karakas, A. I., Lugaro, M., & Gallino, R. 2007, ApJL, 656, L73
Kramida, A., Ralchenko, Y., Reader, J. & N. A. Team 2023, NIST Atomic Spectra Database, v5.11 doi:10.18434/T4W30F
Kurucz, R. 1988, in Transactions of the IAU XXB, ed. M. McNally (Dordrecht: Kluwer), 168
Kurucz, R. L., & Peytremann, E. 1975, Research in Space 362, Smithsonian Institution, Astrophysical Observatory
Ljung, G., Nilsson, H., Asplund, M., & Johansson, S. 2006, A&A, 456, 1181
Malcheva, G., Blagoev, K., Mayo, R., et al. 2006, MNRAS, 367, 754
Menon, A., Karakas, A. I., Lugaro, M., Doherty, C. L., & Ritter, C. 2019, MNRAS, 482, 2320
Moore, C. E. 1972, A Multiplet Table of Astrophysical Interest, Revised Edition: Part I—Table of Multiplets, Part II—Finding List of All Lines in the Table of Multiplets (Gaithersburg, MD: National Institute of Standards and Technology)
Moore, C. E. 1993, in Tables of Spectra of Hydrogen, Carbon, Nitrogen, and Oxygen Atoms and Ions, ed. J. W. Gallagher (Boca Raton, FL: CRC Press),
Pandey, G. 2006, ApJL, 648, L143
Pandey, G., & Reddy, B. E. 2006, MNRAS, 369, 1677
Pandey, G., & Lambert, D. L. 2011, ApJ, 727, 122
Pandey, G., & Lambert, D. L. 2017, ApJ, 847, 127
Pandey, G., Hema, B. P., & Reddy, A. B. S. 2021, ApJ, 921, 52
Pandey, G., Lambert, D. L., Rao, N. K., & Jeffery, C. S. 2004, ApJL, 602, L113
Pandey, G., Lambert, D. L., Jeffery, C. S., & Rao, N. K. 2006, ApJ, 638, 454
Pandey, G., Kameswara Rao, N., Jeffery, C. S., & Lambert, D. L. 2014, ApJ, 793, 76
Pandey, G., Kameswara Rao, N., Lambert, D. L., Jeffery, C. S., & Asplund, M. 2001, MNRAS, 324, 937
Przybilla, N., Fossati, L., & Jeffery, C. S. 2021, RNAAS, 5, 254
Roederer, I. U. 2012, ApJ, 756, 36
Ryde, N., & Lambert, D. L. 2004, A&A, 415, 559
Shultz, M. E., Kochukhov, O., Labadie-Bartz, J., David-Uraz, A., & Owocki, S. P. 2021, MNRAS, 507, 1283
Sriram, S., Kumar, A., Surya, A., et al. 2018, Proc. SPIE, 10702, 107026K
Tisserand, P., Crawford, C. L., Clayton, G. C., et al. 2022, A&A, 667, A83
Tody, D. 1986, Proc. SPIE, 627, 733
Tody, D. 1993, in ASP Conf. Ser. 52, Astronomical Data Analysis Software and Systems II, ed. R. J. Hanisch, R. J. V. Brissenden, & J. Barnes (San Francisco, CA: ASP), 173
Tomkin, J., Edvardsson, B., Lambert, D. L., & Gustafsson, B. 1997, A&A, 327, 587
Warner, B. 1963, MNRAS, 126, 61
Warner, B. 1967, MNRAS, 137, 119
Wiese, W. L., Smith, M. W., & Glennon, B. M. 1966, Atomic Transition Probabilities. Vol.: Hydrogen through Neon. A Critical Data Compilation, NSRDS-NBS 4 (Washington, D.C.: US Department of Commerce, National Bureau of Standards)